Cancer Cell
Article

Ink4a/Arf and Oncogene-Induced Senescence Prevent Tumor Progression during Alternative Colorectal Tumorigenesis

Moritz Bennecke,[1] Lydia Kriegl,[2] Monther Bajbouj,[1] Kristin Retzlaff,[1] Sylvie Robine,[3] Andreas Jung,[2] Melek C. Arkan,[1] Thomas Kirchner,[2] and Florian R. Greten[1,*]
[1]2nd Department of Medicine, Klinikum rechts der Isar, Technical University Munich, 81675 Munich, Germany
[2]Institute of Pathology, Ludwig-Maximilian-University, 80337 Munich, Germany
[3]Morphogenesis and Intracellular Signaling, UMR 144, Institute Curie-CNRS, 75248 Paris cedex 05, France
*Correspondence: florian.greten@lrz.tum.de
DOI 10.1016/j.ccr.2010.06.013

SUMMARY

Colonic cancers with a serrated morphology have been proposed to comprise a molecularly distinct tumor entity following an alternative pathway of genetic alterations independently of *APC* mutations. We demonstrate that intestinal epithelial cell specific expression of oncogenic K-ras^{G12D} in mice induces serrated hyperplasia, which is characterized by p16^{ink4a} overexpression and induction of senescence. Deletion of *Ink4a/Arf* in *K-ras^{G12D}* expressing mice prevents senescence and leads to invasive, metastasizing carcinomas with morphological and molecular alterations comparable to human *KRAS* mutated serrated tumors. Thus, we suggest that oncogenic K-ras represents a key player during an alternative, serrated pathway to colorectal cancer and hence propose RAS-RAF-MEK signaling apart from *APC* as an additional gatekeeper in colorectal tumor development.

INTRODUCTION

Despite significant improvements in prevention, colorectal cancer remains the third most common cancer as well as the third leading cause of cancer-associated death worldwide (Jemal et al., 2009; Kamangar et al., 2006). An exact understanding of the molecular events during carcinogenesis is crucial to develop efficient preventive and therapeutic strategies. The discovery of the genetic basis for familial adenomatous polyposis (FAP), the demonstration that genetic alterations of adenomatous polyposis coli (*APC*) are found in the majority of sporadic colorectal neoplasms (Vogelstein et al., 1988), and the fact that loss of *APC* is sufficient to induce tumorigenesis led to the definition of APC as the ''gatekeeper'' of colonic carcinogenesis (Kinzler and Vogelstein, 1996). *APC* mutations lead to chromosomal instability (CIN) and followed by additional mutations in tumor suppressors and oncogenes along the adenoma-carcinoma sequence ultimately to invasive cancer (Lengauer et al., 1998).

However, accumulating evidence suggests that certain colorectal tumors do not follow this classical pathway and may arise independently of *APC* mutations. Because of their distinct histological and molecular features this group of tumors, which may explain 7.5% of all and 17.5% of proximal colorectal cancers, has been proposed to follow an alternative pathway, the so-called serrated route to cancer (Jass, 2007; Makinen, 2007; Noffsinger, 2009). This class of tumors comprises a morphologically and presumably molecularly heterogenous group ranging from hyperplastic polyps (HP), sessile serrated polyps (SSA), traditional serrated adenomas (TSA), and mixed polyps to serrated carcinoma (Noffsinger, 2009), that all have a sawtooth-like (serrated) infolding of the neoplastic epithelium in common (Makinen, 2007). Further typical characteristics of serrated carcinomas are mucin secretion, absence of ''dirty necrosis,'' lymphocytic infiltration and poor differentiation (Huang et al., 2004; Jass et al., 2002). Because a very large number of activating mutations of either *KRAS* or *BRAF* have been detected as the earliest genetic alterations in serrated lesions, activation of the RAS-RAF-MEK-ERK-MAP axis has been suggested to be the initiating event in serrated carcinogenesis. In contrast to classical colonic tumors that show CIN,

Significance

Initiation of serrated tumors that follow the so-called alternative route to colorectal cancer is presumably caused by *KRAS* or *BRAF* mutations. We present a mouse model that develops colonic tumors that morphologically and molecularly mimics human serrated tumors harboring KRAS mutations. Thus, we provide what we believe to be an important tool for diagnostic and therapeutic studies of serrated cancers and highlight a so far unanticipated relevance of oncogene-induced senescence and *Ink4a/Arf* in colon cancer progression.

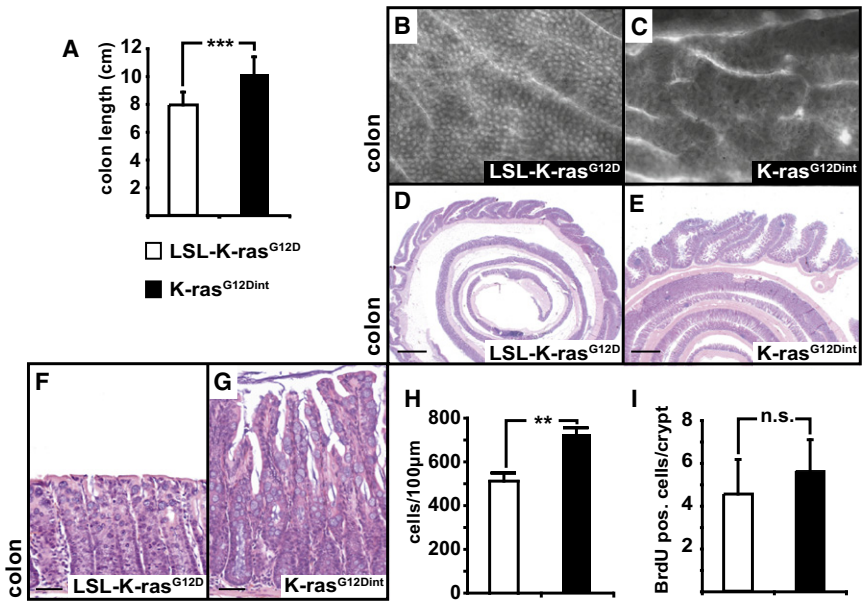

Figure 1. Widespread Serrated Hyperplasia but Lack of Hyperproliferation in K-ras^{G12D} Expressing Colon

(A) Average length of colons along the longitudinal axis in *LSL-K-ras$^{G12D/+}$* (white bar) and *K-ras^{G12Dint}* (black bar) mice. Data are mean ± SE; n ≥ 5; ***p < 0.001 by t test.

(B and C) Whole mount methylene blue stained colon of (B) *LSL-K-ras$^{G12D/+}$* and (C) *K-ras^{G12Dint}* mice. Note that due to the lack of remaining normal crypts, hyperplastic ones are not recognizable as aberrant crypt foci or single polyps.

(D–G) H&E stained sections of (D and F) *LSL-K-ras$^{G12D/+}$* and (E and G) *K-ras^{G12Dint}* mice demonstrating (E) pronounced proximal folds and (mSH, G) crypt hyperplasia in colon of *K-ras^{G12Dint}* mice. Scale bars represent 100 µm (D and E) and 50 µm (F and G).

(H) Epithelial cell number per 100 µm colonic muscularis mucosae and (I) mitotic index in colon of *LSL-K-ras$^{G12D/+}$* (white bars) and *K-ras^{G12Dint}* (black bars) mice.

All animals were analyzed at the age of 16 weeks. Data are mean ± SE; n ≥ 5; **p < 0.01 and not significant (n.s.) by t test. See also Figure S1.

serrated cancers are frequently characterized by a CpG island methylator phenotype (CIMP) and subsequent high-level DNA microsatellite instability (MSI-H) especially when located proximally and associated with *BRAF* mutations (Cunningham and Riddell, 2006). However, *KRAS* mutated tumors are more frequently CIMP negative and MSI-L/MSS. A further mechanism proposed to play a key role in the pathogenesis of these tumors seems to comprise loss of the DNA mismatch repair gene *hMLH1* or the DNA repair gene O^6-methylguanine DNA methyltransferase (*MGMT*) (Jass et al., 2002). Furthermore, it has been speculated that senescence might occur in early tumor stages preventing tumor progression (Jass, 2007), however, functional evidence for this hypothesis is lacking. To test whether we could recapitulate development of serrated tumorigenesis in mice and to analyze the molecular events required for progression to cancer, we examined animals expressing oncogenic K-ras^{G12D} specifically in enterocytes.

RESULTS

Enterocyte-Specific Expression of K-ras^{G12D} Leads to Formation of Colonic Serrated Lesions

To establish whether intestinal epithelial cell (IEC)-specific expression of oncogenic *K-ras^{G12D}* would allow serrated tumor formation, we crossed *villin*-Cre mice (Madison et al., 2002) to *LSL-K-ras$^{G12D/+}$* mice (Jackson et al., 2001). The resulting mice, termed *K-ras^{G12Dint}*, were born at the expected Mendelian ratio and did not display any overt developmental defects or weight differences (data not shown). Macroscopic analysis of K-ras^{G12D} expressing intestines at 16 weeks of age displayed a significant elongation of their large intestine (Figure 1A). In contrast to *LSL-K-ras$^{G12D/+}$* control animals, whole mount analysis of methylene-blue stained colon from *K-ras^{G12Dint}* mice revealed irregular crypt morphology (Figures 1B and 1C). Histological analysis of *K-ras^{G12Dint}* mice demonstrated occurrence of pronounced proximal colonic folds (Figures 1D and 1E). More importantly, in *K-ras^{G12Dint}* colons we detected the expected serrated, hyperplastic transformation (Figures 1F and 1G), which was not patchy, but rather uniformly spread along the whole large intestine affecting nearly every single crypt. These hyperplastic crypts closely resembled the histology found in human premalignant lesions of the serrated route (see Figure S1 available online) and we therefore refer to this histology as ''murine serrated hyperplasia'' (mSH). Development of mSH occurred with a 100% penetrance and independently of gender or genetic background (C57BL/6;129 or after backcrossing to FVB/N for four generations). Despite the marked hyperplasia in *K-ras^{G12Dint}* mice (defined by a significantly increased cell number/100 µm muscularis mucosae, Figure 1H), we could not observe a difference in the colonic mitotic index determined by BrdU-labeling compared to littermate control mice (Figure 1I), or in apoptotic index examined by staining for active caspase 3 (data not shown).

In small intestine (SI) of *K-ras^{G12Dint}* mice length was significantly increased along the longitudinal as well as the vertical axis (Figure S2). In contrast to the colon of these mice, however, villus elongation was associated with a higher proliferation and migration rate determined by BrdU incorporation (Figure S2). Further histological analysis of mutant SI revealed a high incidence of villus branching and consistent with elongation along the longitudinal axis, we frequently observed crypt fission (Figure S2).

To test whether endogenous expression of K-ras^{G12D} was sufficient to promote colonic tumor growth along the serrated route we monitored *K-ras^{G12Dint}* up to 17 months. However, in none of the *K-ras^{G12Dint}* expressing colons, progression of the mSH into more advanced tumor stages or carcinomas was observed. In contrast, but consistent with a hyperproliferative phenotype in the small intestine, 25% of *K-ras^{G12Dint}* animals (7/28) developed a single adenoma in the duodenum/jejunum after 1 year (Figure S2 and Table S1).

Collectively, the endogenous expression of oncogenic K-ras led to significant albeit distinct alterations in the architecture of

both small and large intestine. Whereas in small intestinal IEC K-ras^{G12D} induced a persistent hyperproliferation and occasionally development of adenomas, mutant colon was characterized by the initiation of a presumably growth-arrested, serrated hyperplasia, which, however, did not progress into malignant tumors.

Oncogene-Induced Senescence Is Responsible for Growth Arrest of Colonic mSH

Oncogene-induced senescence (OIS) is a form of stable growth arrest that can be induced by overexpression of oncogenes in cultured cells (Collado and Serrano, 2010). OIS can occur in vivo in various premalignant lesions of malignant melanoma, lymphoma, prostate, and lung cancer presumably having a tumor suppressive function (Braig et al., 2005; Chen et al., 2005; Collado et al., 2005; Michaloglou et al., 2005). Oncogenic K-ras mediated Erk activation is one of the main inducers of senescence (Mooi and Peeper, 2006), which might be the underlying cause for the block of progression in mSH. To test this, we isolated IEC for biochemical analysis. First, activation of K-ras in mutant IEC was confirmed by pull-down assay of GTP-bound Ras (Figure 2A). This led to the expected phosphorylation of Erk1/2 without affecting total protein levels of Erk (Figure 2B). In contrast, activation of other downstream effectors of Ras, such as Akt and Ral (Malumbres and Barbacid, 2003) remained either unchanged or undetectable in colonocytes of mice of either genotype, respectively (Figures 2C and 2D). Furthermore, we did not observe any activation of the other MAP-kinases p38 or JNK (Figures 2E and 2F), which had been found to be upregulated in K-ras^{G12D} expressing lungs (Lee et al., 2002), indicating that endogenous expression of K-ras^{G12D} in IEC primarily activates Erk1/2. To test, whether K-ras mediated Erk-activation might lead to senescence, we examined enzymatic activity of senescence-associated (SA) β-galactosidase, a marker indicating senescence both in vitro and in vivo (Dimri et al., 1995), in colons of *K-ras^{G12Dint}* mice and littermates. As hypothesized, mSH exhibited strikingly elevated SA-β-galactosidase activity, which was not observed in untransformed colons of control littermates (Figures 2G and 2H). The presence of OIS was further supported by upregulation of mRNA encoding the senescence marker Dec1 (Figure 2I) as well as increased p16^{ink4a} mRNA and protein levels in isolated colonic IEC of *K-ras^{G12Dint}* mice (Figures 2I and 2J). However, we could not detect upregulation of p19^{Arf} or p53 mRNA (Figure 2I) or protein levels (Figure 2J and data not shown). In contrast, analysis of small intestinal IEC displayed also selective phosphorylation of Erk, but in line with the observed hyperproliferation in K-ras^{G12D} expressing SI, neither upregulation of p16^{ink4a} mRNA nor induction of senescence were observed (Figure S2).

Unlike our mouse model that exhibits oncogenic K-ras starting from embryonic day 12.5 dpc (Madison et al., 2002), tumor-initiating mutations in human colon occur during adulthood. To confirm that activation of oncogenic Kras in murine adult IEC could still induce serrated hyperplasia, we crossed LSL-K-ras^{G12D} to inducible *villin-cre*ER^{T2}/*LSL-K-ras$^{G12D/+}$* mice (el Marjou et al., 2004). Similarly to *K-ras^{G12Dint}* mice, activation of Cre-recombinase in adult *villin-cre*ER^{T2}/*LSL-K-ras$^{G12D/+}$* mice led to mSH development, upregulation of p16^{ink4a} and occurrence of OIS within 21 days after tamoxifen application (Figure S3 and data not shown). Although an increased BrdU incorporation was readily detectable within 6 days on first

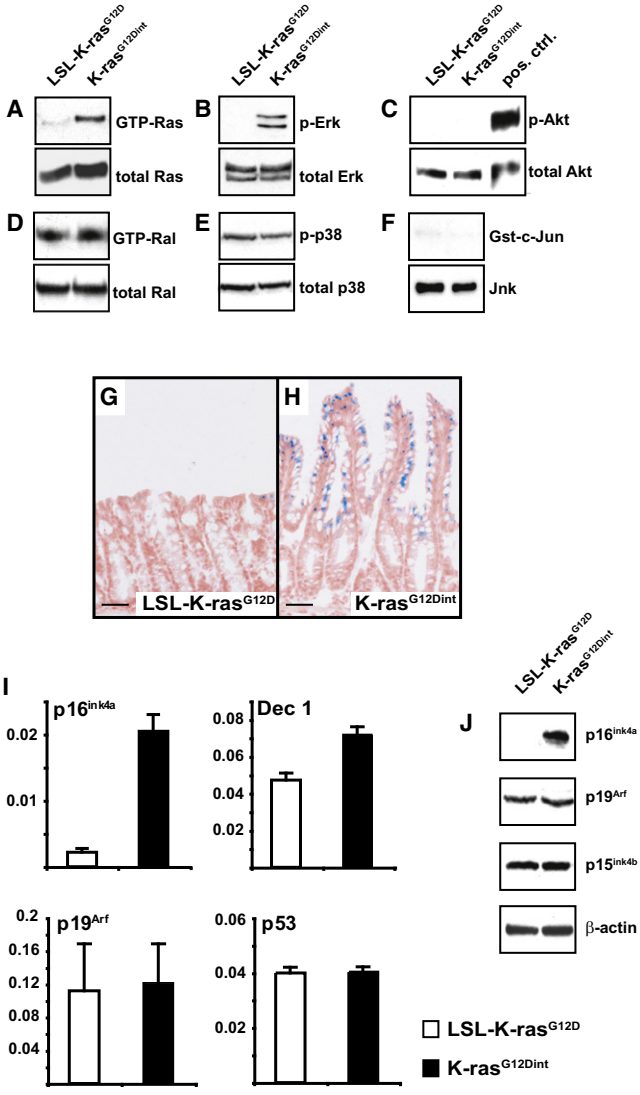

Figure 2. Colonic mSH Are Characterized by Upregulation of p16^{ink4a} and OIS

(A–F) Biochemical analysis of isolated colonic enterocytes at 16 weeks. Activation assay of (A) Ras and (D) Ral. Immunoblot analysis of (B) Erk, (C) Akt, and (E) p38 activation as well as immune complex kinase assay of (F) Jnk.

(G and H) Demonstration of OIS in mSH by SA-β-galactosidase assay on frozen colonic sections of (G) *LSL-K-ras$^{G12D/+}$* and (H) *K-ras^{G12Dint}* mice. Scale bars represent 50 μm.

(I) Relative levels of p16^{ink4a}, p19^{Arf}, Dec1, and p53 mRNA levels in *LSL-K-ras$^{G12D/+}$* (white bars) and *K-ras^{G12Dint}* (black bars) mice. mRNA levels represent the mean ± SE of a minimum of three animals of each genotype.

(J) Immunoblot analysis of p16^{ink4a}, p19^{Arf}, p15^{ink4b}, and β-actin. See also Figure S2.

tamoxifen administration in *villin-cre^{ERT2}/LSL-K-ras$^{G12D/+}$* colon, it was absent after 21 days (Figure S3) resembling the situation in *K-ras^{G12Dint}* mice.

Loss of *Ink4a/Arf* Leads to Metastasizing Serrated Cancer in *K-ras^{G12Dint}* Mice

To functionally confirm the importance of OIS for the growth arrest of mSH, we crossed *K-ras^{G12Dint}* mice to *Ink4a/Arf*

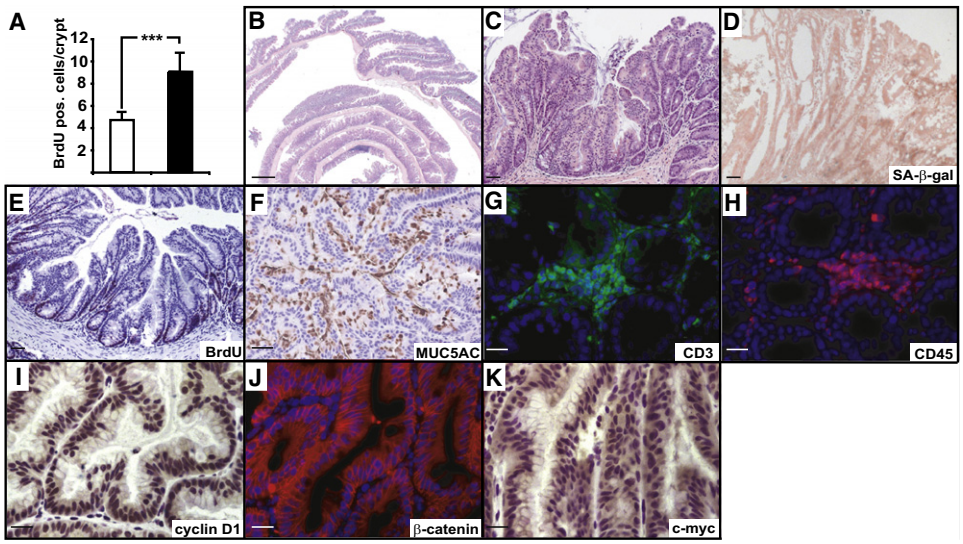

Figure 3. Loss of *Ink4a/Arf* Allows Hyperproliferation and Tumor Progression in *K-ras*^{G12Dint} Mice

(A) Mitotic index in *Ink4a/Arf*$^{-/-}$ (white bar) and *K-ras*^{G12Dint}*/Ink4a/Arf*$^{-/-}$ (black bar) mice at 12 weeks; Data are mean ± SE; n ≥ 4; ***p < 0.001 by t test.

(B and C) H&E stained sections of mice displaying (B) further deepening of proximal folds and (C) formation of traditional serrated adenoma. Scale bars represent 100 μm (B) and 50 μm (C).

(D) SA-β-galactosidase assay demonstrating loss of OIS. Scale bar represents 50 μm.

(E–K) Immunohistochemical and immunofluorescent staining of (E) BrdU, (F) MUC5AC, (G) CD3, (H) CD45, (I) cyclin D1, (J) β-catenin, and (K) c-*myc*. Scale bars represent 50 μm (F–H) and 20 μm (I–K). See also Figure S3 and Table S1.

deficient mice (Serrano et al., 1996) to generate *K-ras*^{G12Dint}*/Ink4a/Arf*$^{-/-}$ (resulting in IEC-specific activation of K-ras^{G12D} and whole body deletion of *Ink4a/Arf*). Consistent with the upregulation of p16^{ink4a} in colonic but not small intestinal *K-ras*^{G12Dint} IEC, deletion of *Ink4a/Arf* induced colonic hyperproliferation (Figure 3A), but left small intestinal morphology of *K-ras*^{G12Dint} mice unaffected. Furthermore, elongation of colonic proximal folds was more pronounced on *Ink4a/Arf*-loss than in *K-ras*^{G12Dint} mice (Figure 3B, compare to Figure 1E). More importantly, within 12 weeks, in more than 50% of *K-ras*^{G12Dint}*/Ink4a/Arf*$^{-/-}$ mice (17/32), hyperplasia had progressed into tumors that resembled traditional serrated adenomas (Figure 3C and Figure S3) that were located exclusively in the proximal colon (Table S1).

Loss of Ink4a/Arf-mediated senescence in murine serrated adenomas was confirmed by the lack of SA-β-gal activity (Figure 3D). Proliferating cells, determined by BrdU incorporation, were predominantly located in the lower half of crypts (Figure 3E). Further immunohistochemical analysis of these adenomas in *K-ras*^{G12Dint}*/Ink4a/Arf*$^{-/-}$ mice revealed aberrant expression of MUC5AC (Figure 3F), suggesting differentiation of mucous cells toward gastric surface mucous cells. Moreover, we detected significant lymphocytic infiltration along the lamina propria and surrounding the adenomatous epithelia determined by immunofluorescent staining against CD3 and CD45 (Figures 3G and 3H). While epithelial cells stained positive for cyclin D1 (Figure 3I), β-catenin showed a membrane bound expression pattern (Figure 3J) and these cells retained APC expression (data not shown). Only few cells expressed nuclear c-*myc* (Figure 3K), collectively indicating that these tumors did not show activation of the Wnt pathway. Remarkably, within 12 weeks in 76% of the *K-ras*^{G12Dint}*/Ink4a/Arf*$^{-/-}$ mice (13/17) with serrated adenomas, tumors had developed into fully invasive adenocarcinomas (Figures 4A–4C and Figure S4). These cancers were exclusively located in the proximal colon and displayed a highly proliferative and poorly differentiated phenotype (Figure 4D). Expression of cytokeratin (CK) 8/18 confirmed the epithelial origin of these invasive cells (Figure 4E). Surprisingly, expression of p53 was consistently positive in all colonic serrated cancers (Figure 4F), however, we were not able to detect any mutations when we sequenced exons 5–8 of *Tp53* in laser-microdissected tumor DNA. In agreement with a membranous expression of β-catenin, we also did not detect any mutations in exon 3 of β-catenin that could lead to stabilization of β-catenin. More importantly, 62% of these invasive cancers (8/13) had metastasized to the lung (Figure 4G and Table S1). Intestinal origin of these metastases was confirmed by staining for CK 20 (Figure 4H).

Notably, by 12 weeks the majority of *K-ras*^{G12Dint}*/Ink4a/Arf*$^{-/-}$ mice became moribund showing signs of severe respiratory distress. We therefore analyzed lungs of these animals and detected also lung tumors in mice that did not have invasive serrated cancer suggesting the existence of primary lung adenomas. This was confirmed by positive immunohistochemical staining for TTF-1, a marker, which is specifically expressed in primary lung tumors, but not in colonic metastases and negative staining for CK7 (Figure S4). Recombination of the mutated K-ras allele in primary lung adenomas was confirmed by PCR analysis of DNA isolated from laser-capture microdissected tumor tissue (data not shown). The early occurrence of primary lung tumors limited a longer monitoring of *K-ras*^{G12Dint}*/Ink4a/Arf*$^{-/-}$ mice.

To functionally examine the role of p53 in serrated tumor development, we crossed *K-ras*^{G12Dint} animals to conditional

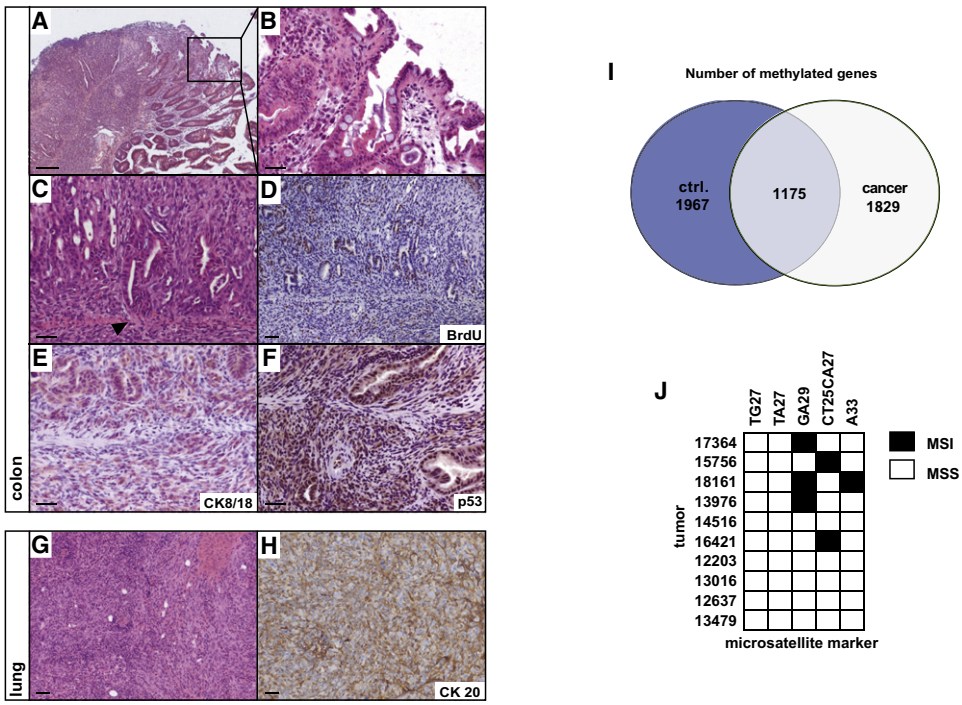

Figure 4. Rapid Development of CIMP Negative and MSS-L/MSS Serrated Adenocarcinomas that Metastasize to the Lung in *Ink4a/Arf*-Deficient *K-ras*^{G12Dint} Mice

(A–C) H&E stained sections of invasive carcinoma in *K-ras*^{G12Dint}/*Ink4a/Arf*$^{-/-}$ mice with serration at the luminal surface (B) and invasion of epithelia (arrowhead, C) through the lamina propria into the submucosa. Scale bars represent 200 μm (A) and 50 μm (B and C).

(D–F) Immunohistochemical staining of (D) BrdU, (E) CK8/18, and (F) p53. Scale bars represent 50 μm.

(G) H&E stained section of a lung metastasis of the primary tumor shown in (A). Scale bar represents 50 μm.

(H) Immunohistochemical staining of CK20 confirming intestinal origin of metastasis. Scale bar represents 50 μm.

(I) Venn diagram displaying the average number of methylated genes in colonic DNA isolated from control animals or serrated *K-ras*^{G12Dint}/*Ink4a/Arf*$^{-/-}$ cancers ($n \geq 3$ of each genotype).

(J) Summary of the microsatellite stability (MSI) analysis comparing *K-ras*^{G12Dint}/*Ink4a/Arf*$^{-/-}$ cancers to healthy tissues from the same animals using five different microsatellite repeat markers; white box indicates microsatellite stability (MSS), black box indicates MSI. See also Figure S4.

Trp53 mice (Jonkers et al., 2001) to generate *K-ras*^{G12Dint}/*Trp53*$^{\Delta int}$ mice (resulting in specific activation of K-ras^{G12D} and concomitant deletion of *Trp53* restricted to enterocytes). Although about one-third of *K-ras*^{G12Dint}/*Trp53*$^{\Delta int}$ mice (4/11) developed small intestinal tumors within 1 year, we could not observe tumor progression beyond the stage of hyperplasia in the colon of these double mutants even when we monitored them up to 12 months (Table S1). This was in agreement with a missing upregulation of p19^{Arf} or p53 in colonic mSH in *K-ras*^{G12Dint} mice (Figures 2I and 2J). Importantly, also additional IEC-restricted deletion of *Trp53* in *K-ras*^{G12Dint}/*Ink4a/Arf*$^{-/-}$ mice did not accelerate cancer development, despite the nuclear accumulation of p53 in *K-ras*^{G12Dint}/*Ink4a/Arf*$^{-/-}$ cancers (data not shown). Collectively, these data supported the notion that the p16^{ink4a}/Rb pathway but not the p19^{Arf}/p53 pathway antagonizes colonic serrated tumor development.

Murine Serrated Cancers Are CIMP Negative and MSI-L/MSS

Human serrated tumors harboring *KRAS* mutations frequently exhibit a CIMP-low/CIMP-negative and microsatellite stable or low profile (MSS/MSI-L) in contrast to tumors with *BRAF* mutations that are characterized by extensive methylation of certain CpG islands (CIMP-high) and microsatellite instability (MSI-H) (Jass, 2007). To determine methylation and microsatellite status of *K-ras*^{G12Dint}/*Ink4a/Arf*$^{-/-}$ serrated cancers, we enriched methylated DNA by MeDIP (methylated DNA immunoprecipitation) from *K-ras*^{G12Dint}/*Ink4a/Arf*$^{-/-}$ tumor samples and control animals before hybridization on a NimbleGen 385K MM8 RefSeq promoter array. Whereas a large number of genes were commonly methylated in both groups, the overall number of methylated genes was higher in DNA from control mice (Figure 4I). None of the classic CIMP markers (*Mint1*, *Mint2*, *Mint31*, *Mlh1*) or the more recently established markers defining CIMP (*Igf2*, *Cacna1g*, *Neurog1*, *Runx3*, *Socs1*) (Weisenberger et al., 2006) was methylated in control or tumor DNA indicating that *K-ras*^{G12Dint}/*Ink4a/Arf*$^{-/-}$ cancers were CIMP negative. In addition, mRNA levels encoding these various markers were not significantly different in tumors compared to controls (data not shown), supporting the notion that *K-ras*^{G12Dint}/*Ink4a/Arf*$^{-/-}$ tumors were indeed CIMP-negative.

To assess whether murine serrated cancers displayed MSI, we compared DNA from microdissected tumors to DNA isolated from tumor-free livers of the same animals using a panel of five microsatellite repeat markers faithfully detecting MSI (Kabbarah et al., 2003). The majority of tumors was either MSI-L (4/10) or

MSS (5/10) and only 1 of 10 analyzed tumors (no. 18161) fulfilled the criteria for MSI-H (Boland et al., 1998) (Figure 4J).

Collectively, these data demonstrated that the murine K-ras mutated cancers were CIMP-negative and MSS-L/MSS, thus closely resembling the molecular characteristics of human *KRAS* mutated serrated polyps and carcinomas.

Activation of Wnt Signaling Is Not Required for Murine K-ras^{G12D} Initiated Serrated Tumor Growth

Serrated adenocarcinomas are considered to develop independently of Wnt activation in the majority of cases. Accordingly, serrated tumors in *K-ras*^{G12Dint}/*Ink4a/Arf*$^{-/-}$ mice did not show any activating *Ctnnb* mutations, loss of APC expression or pronounced nuclear expression of β-catenin. To functionally confirm that serrated tumor growth occurred independently of Wnt activation, we injected *K-ras*^{G12Dint} mice six times intraperitoneally (i.p.) once a week with azoxymethane (AOM). AOM is a procarcinogen, which on metabolic activation leads to the formation of O^6-methyl-guanine-adducts and is commonly used in animal models to induce classical colonic tumors (Boivin et al., 2003). AOM is known to initiate mutations in exon 3 of *Ctnnb*, thereby stabilizing β-catenin and subsequently activating Wnt signaling (Greten et al., 2004). Because AOM primarily induces colonic tumors we preferred this model to genetic models of sporadic tumorigenesis, such as *Apc* mutants, which primarily develop small intestinal tumors. Sixteen weeks after the first AOM injection animals were sacrificed and tumor incidence as well as tumor morphology was determined. In contrast to the serrated cancers that developed in *K-ras*^{G12Dint}/*Ink4a/Arf*$^{-/-}$ mice, all of the AOM-induced adenomas were located in the distal colon, which is the typical location of tumors following the classical pathway. However, *K-ras*^{G12Dint} mice developed ~13-fold more tumors compared to control littermates (Figure 5A) in agreement with the notion that oncogenic K-ras enhances classical colon cancer progression (Haigis et al., 2008; Janssen et al., 2006). The vast majority of AOM-induced tumors were tubular and well-differentiated, displayed low to moderate dysplasia and none of them was invasive (Figures 5B and 5C). Sequence analysis of exon 3 of *Ctnnb* in DNA isolated from microdissected tumor tissue revealed activating mutations in tumors of either genotype (data not shown). Accordingly, activation of Wnt signaling was further confirmed by immunohistochemical stainings against β-catenin and its downstream target c-*myc*, which both demonstrated nuclear localization in tumors of either genotype (Figures 5D–5G). To establish that AOM-induced tumors were also molecularly distinct from serrated cancers, we performed comparative gene expression analysis on RNA samples isolated from serrated cancers of *K-ras*^{G12Dint}/*Ink4a/Arf*$^{-/-}$ mice and classical, AOM-induced tumors from *K-ras*^{G12Dint} and *LSL-K-ras*$^{G12D/+}$ mice. Hierarchical clustering of the samples revealed a significantly different expression profile in serrated cancers compared to AOM-induced tumors (Figure 5H). When we performed gene set enrichment analysis (GSEA) to compare these gene expression profiles to that of mice with an IEC-restricted deletion of *Apc* (Sansom et al., 2007), the AOM-induced tumors but not the serrated tumors demonstrated a high enrichment with the "Wnt signature" that is reminiscent of classical tumors (Figure 5I) (Kaiser et al., 2007).

Recently, a gene expression profiling study demonstrated that human serrated cancers comprise a distinct molecular subclass of colon cancers and several specific biomarkers were identified (Laiho et al., 2007). When comparing serrated cancers to conventional colon cancers it was suggested that upregulation of *HIF1α* and its downstream target *BNIP3L* as well as downregulation of *EPHB2* and *PTCH* could be specifically found in serrated cancers. Although it is not clear whether the serrated cancers in this study contained *KRAS* or *BRAF* mutations, we compared RNA expression levels of these biomarkers in murine AOM-induced tumors and serrated cancers. Similarly to human cancers, RNA levels coding for EphB2 were higher in classical AOM-induced tumors whereas *Hif-1α* and *Bnip3l* mRNAs were markedly upregulated in murine serrated cancers, yet expression of *Ptch* remained unchanged (Figure 5J and data not shown). Immunohistochemical analysis confirmed the reciprocal expression pattern of EphB2 and Hif-1α in tumor epithelium of classical and serrated tumors (Figures 5K–5N).

Human *KRAS* Mutated Serrated Adenomas Show OIS and Express High Levels of p16^{INK4A}

Having established the importance of OIS and *Ink4a/Arf* in murine serrated tumor development, we wanted to examine whether senescence and p16^{INK4A} upregulation might be observed in human *KRAS* associated serrated carcinogenesis as well. Therefore, we obtained during routine colonoscopy 18 hyperplastic polyps (HP), of which four contained a *KRAS* (codon 12) mutation and as hypothesized, three of them revealed a marked positive expression of SA-β-gal indicating OIS in HP (Figure 6A). Furthermore, this was accompanied by p16^{INK4A} expression, which was undetectable in unaffected, healthy mucosa (Figures 6C and 6D). To examine whether p16^{INK4A} upregulation was a general phenomenon commonly found in *KRAS* mutated benign serrated lesions and whether tumor progression was associated with loss of p16^{INK4A}, we extended our analysis to a cohort of 93 serrated tumors comprising hyperplastic polyps, sessile serrated adenomas, traditional serrated adenomas, early invasive serrated adenocarcinomas within a serrated adenoma and also advanced serrated adenocarcinomas with metastasis. We screened this cohort for the presence of *KRAS* (codon 12, 13) or *BRAF* (V600E) mutations and identified 13 serrated tumors that contained mutated *KRAS* (Table 1). Independently of tumor stage and grade of intraepithelial neoplasia (dysplasia) all 13 *KRAS* mutated tumors were MSS, expressed MLH1 and except two cases displayed membranous β-catenin expression indicating normal Wnt signaling (Table 1). In nearly all samples we could detect robust expression of p16^{INK4A} that increased with degree of intraepithelial neoplasia (dysplasia), whereas p14^{ARF} was not expressed (Figures 7A–7D). However, in three of four tumors that showed signs of invasion p16^{INK4A} expression was selectively reduced at the infiltrative front of invasion and correlated inversely with expression of the proliferation marker Ki67 (Figures 7E and 7F). In one advanced adenocarcinoma with metastasis, p16^{INK4A} expression was completely lost. Decreased expression or loss of p16^{INK4A} was in most cases associated with *CDKN2A* promoter methylation. Because we had observed nuclear accumulation of p53 in murine advanced serrated tumors, we wanted to examine whether we could recapitulate this unexpected finding in human samples as well. Intriguingly, in almost all invasive cancers we found nuclear accumulation of p53. Although in various cancers

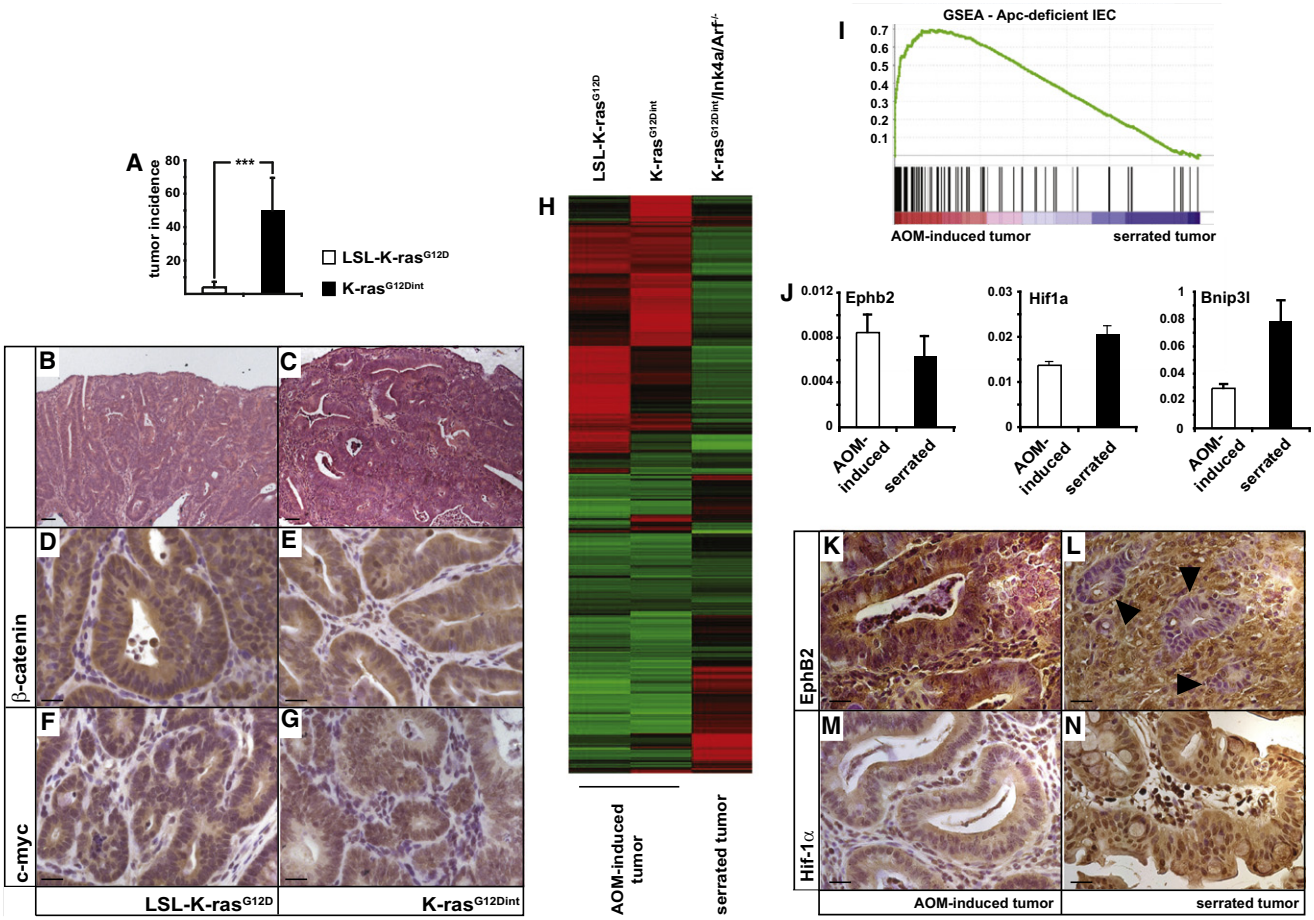

Figure 5. Oncogenic K-ras and Wnt Activation Cooperate in Classical but Not in Alternative Colon Carcinogenesis

(A) Tumor incidence in *LSL-K-ras*$^{G12D/+}$ (white bar, n = 6) and *K-ras*^{G12Dint} (black bar, n = 5) mice 16 weeks after the first of six AOM injections. Data are mean ± SE; ***p < 0.001 by t test.

(B and C) H&E stained sections of adenomas in (B) *LSL-K-ras*$^{G12D/+}$ and (C) *K-ras*^{G12Dint} mice.

(D–G) Immunohistochemical staining of (D and E) β-catenin and (F and G) c-*myc*.

(H) Two to three whole colonic tumor RNA samples from individual mice were analyzed by Affymetrix MOE430A 2.0 expression profiling. RMA-normalized expression values were subjected to statistical analysis (Limma F test p value < 0.005) and filtered for absolute and relative changes between average expression values (max/min > 2, max-min > 80). The resulting 1309 probe sets were *Z*-score normalized and subjected to hierarchical clustering; red indicates high expression, green indicates low expression.

(I) GSEA analysis comparing classical AOM-induced tumors and serrated cancers reveals high similarity of AOM-induced tumors with *Apc*-deficient IEC. Normalized enrichment score: 2.83; p < 0.001.

(J) Relative levels of Ephb2, Hif-1α, and Bnip3l in classical AOM-induced tumors (white bars) and serrated cancers (black bars). mRNA levels represent the mean ± SE of a minimum of three animals of each genotype.

(K–N) Immunohistochemical staining of (K, L) EphB2 and (M, N) Hif-1α in AOM-induced tumors and serrated cancers. In classical tumors epithelial cells express EphB2 (K), but in serrated cancers only stromal cells are positive for EphB2, whereas tumor epithelia (arrowheads) remain negative (L). In contrast, Hif-1α displays strong nuclear staining in (N) serrated tumor epithelia but not in (M) classical AOM-induced tumors. All scale bars represent 50 μm.

increased nuclear p53 accumulation is frequently caused by *TP53* mutations (Greenblatt et al., 1994), we could not detect any mutations in the most commonly affected exons 5–8 of *TP53*, resembling the situation in murine serrated cancers.

DISCUSSION

The majority of nonhereditary colorectal cancers follow a well-defined tumor progression model involving APC mutation as an initiating event. Mutation of K-ras occurs at later stages and is supposedly not sufficient to initiate classical colonic tumorigenesis per se. We provide what we believe to be genetic evidence that enterocyte specific expression of oncogenic K-ras in mice can induce widespread colonic lesions that morphologically resemble benign human serrated polyps. Our results therefore support the hypothesis that indeed activation of the RAS-RAF-MEK-ERK cascade may be the initiating event in human serrated colorectal tumors.

Oncogene induced senescence has been suggested to have a tumor suppressive function in a variety of different tumors (Collado and Serrano, 2010). Although neither in primary human colonic tissue nor in experimental models of colorectal cancer

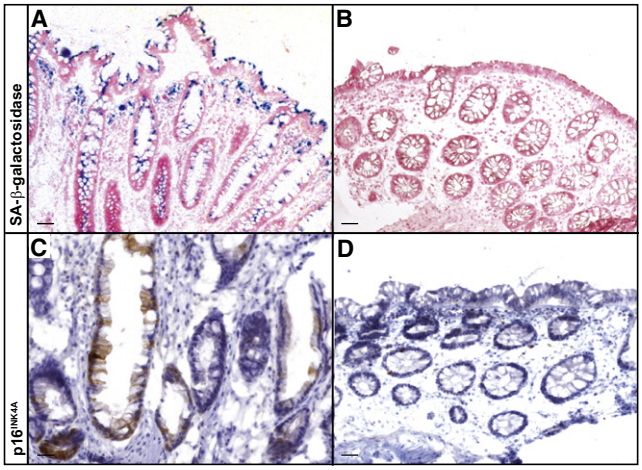

Figure 6. Human *KRAS* Mutated Benign Serrated Polyps Display OIS and Express p16^{INK4A}

(A and B) Positive staining for SA-β-gal indicating existence of OIS in a (A) *KRAS* mutated hyperplastic polyp, but not in (B) healthy mucosa. Scale bars represent 100 μm.

(C and D) Expression of p16^{INK4A} in (C) the same SA-β-gal positive hyperplastic polyp, but not in (D) healthy mucosa. Scale bars represent 50 μm.

senescence has been confirmed yet, OIS may provide a potential molecular mechanism explaining the rare progression of benign early, serrated lesions toward serrated adenocarcinoma. Indeed, we provide evidence that OIS developed in both hyperplastic mutant mouse tissue as well as in human serrated polyps and this was paralleled by upregulation of p16. Similarly to tumor progression in mice that was dependent on loss of *Ink4a/Arf*, p16^{INK4A} expression was either completely absent or lost at the infiltrating front of invasion in the majority of human invasive carcinomas. Furthermore, in tumors that did not express or displayed a reduced p16^{INK4A} expression, *CDKN2A* promoter methylation was commonly confirmed. Although we cannot rule out that loss of *Ink4a/Arf* in stromal cells might affect tumor progression in mice, in light of the findings in human tissues our data strongly support the concept that OIS and p16 upregulation confer tumor suppressive effects during serrated tumorigenesis and suggest that loss of Ink4a/Arf could be one key mechanism required to overcome growth arrest in mutated cells. Because only ~50% of *K-ras^{G12Dint}/Ink4a/Arf$^{-/-}$* mice developed adenomas and carcinomas, presumably additional genetic events are required for serrated tumor progression apart from *Ink4a/Arf* loss. Based on our results obtained with the AOM-model, which shifted the tumor type toward classical tumorigenesis, activation of Wnt signaling does not seem to play a major role in serrated cancer development. Accordingly *APC* or *CTNNB* mutations are found infrequently in human serrated polyps. However, one potentially important candidate could be *Mgmt*, which is often found inactivated in *KRAS* initiated serrated tumorigenesis (Jass, 2007). Although in *K-ras^{G12Dint}* mice Mgmt expression was retained at all stages, it will still be interesting to functionally examine the role of *Mgmt* as well as to identify other so far unknown genes involved in serrated tumor progression in these mice.

The mouse model we describe very closely mimics human pathology and demonstrates many features of human serrated polyps, i.e., proximal location, aberrant expression of gastric mucous markers, lymphocytic infiltration and bottom-up morphogenesis (Jass et al., 2002). Because serrated polyps comprise a morphologically and molecularly heterogenous group of tumors, we restricted our comparative analysis to human *KRAS* mutated serrated lesions. Intriguingly, in addition to the phenotypic similarities also the molecular alterations were strikingly similar between our mouse model and the human tumors. However, considering the fact that *BRAF* mutations

Table 1. Summary of Morphological and Molecular Properties of 13 Human KRAS Mutated Serrated Tumors

Tumor Type	*KRAS* Mutation	*BRAF* Mutation	MSS	MLH1	MGMT	Nuclear β-Catenin	p14^{ARF}	p16^{INK4A}	*CDKN2A* Prom. Methyl.	Nuclear p53	*TP53* Mutation
HP	+	–	+	+	+	–	–	–	+	–	–
SSA	+	–	+	+	+	–	–	+	+	–	–
TSA	+	–	+	+	+	–	–	+++	–	–	–
TSA	+	–	+	+	+	–	–	+++	–	–	–
TSA	+	–	+	+	+	–	–	+++	–	–	–
TSA	+	–	+	+	+	–	–	++	+	–	–
TSA	+	–	+	+	+	–	–	++	+	–	–
Early inv. carc. in TSA	+	–	+	+	+	–	–	+++/–	–	+	–
Early inv. carc. in TSA	+	–	+	+	+	–	–	+++/–	+	–	–
Early inv. carc. in TSA	+	–	+	+	+	–	–	+++/–	–	+	–
Serr. carcinoma	+	–	+	+	–	+	–	+++	–	+	–
Serr. carcinoma	+	–	+	+	+	+	–	+/–	+	+	–
Adv. serr. carcinoma	+	–	+	+	–	–	–	–	+	+	–

Adv. serr. carcinoma, advanced serrated carcinoma with metastasis; HP, hyperplastic polyp; inv. carc., invasive carcinoma; prom. methyl., promoter methylation; serr. carcinoma, serrated carcinoma; SSA, sessile serrated adenoma; TSA, traditional serrated adenoma. Degree of p16^{INK4A} expression is shown as follows: +, low expression; ++, moderate expression; +++, strong expression; +++/–, strong expression with loss in early invasive carcinoma.

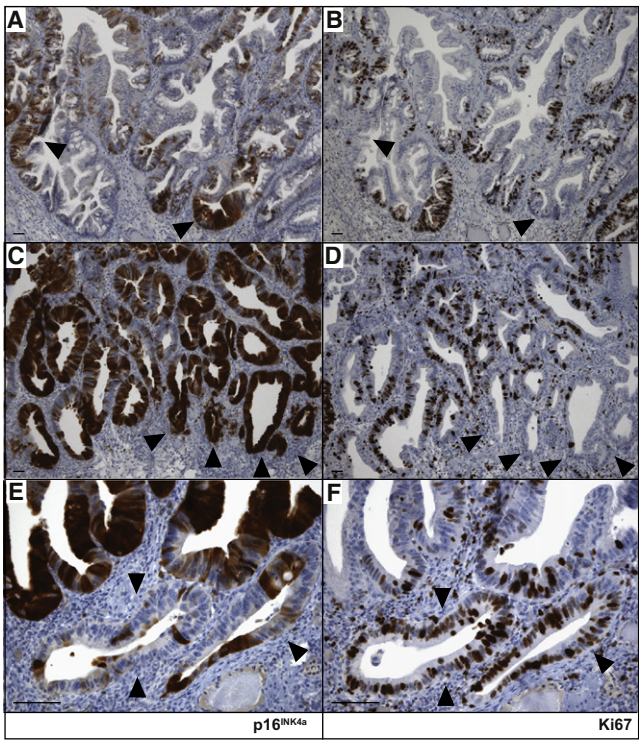

Figure 7. Expression of p16 Increases with Degree of Dysplasia in Human Serrated Polyps but Is Reduced in Early Invasive Carcinoma and Correlates Inversely with Ki67 Expression

(A and B) Moderate $p16^{INK4A}$ expression (A) and inverse expression pattern of Ki67 (B) in *KRAS* mutated traditional serrated adenoma (arrowheads).

(C and D) Strong $p16^{INK4A}$ expression in areas of serrated high-grade intraepithelial neoplasia (dysplasia) (C, arrowheads) inversely correlates with Ki67 expression (D, arrowheads) in serial sections in the area of an early invasive carcinoma within a sessile serrated adenoma.

(E and F) Reduced $p16^{INK4A}$ expression (E, arrowheads) and corresponding increased Ki67 expression (F, arrowheads) in the infiltrating neoplastic cells. All scale bars represent 50 μm.

occur more frequently than *KRAS* mutations in human serrated tumorigenesis, we cannot exclude that our results might be relevant for the subgroup of KRAS-mutated serrated tumors only. Nevertheless, OIS and $p16^{INK4A}$ could have an important function for the early stages of the alternative pathway to colon cancer in general since a marked $p16^{INK4A}$ expression was also detectable in a substantial number of *BRAF* mutated human serrated polyps (L.K. and T.K., unpublished data).

Our results demonstrate a highly pronounced cell type specificity of oncogenic K-ras and unravel a clear difference between small and large intestinal function of K-ras. Small intestinal epithelial cells did not show OIS, Dec1, or p16 upregulation, but they were characterized by persistent hyperproliferation and the occurrence of sporadic tumors after 1 year. Consequently, no small intestinal tumors were observed on loss of *Ink4a/Arf*. In contrast, $K\text{-}ras^{G12D}$ expressing colon was characterized by development of OIS that presumably occurred after an initial brief period of hyperproliferation (compare proliferation rates in inducible *villin-cre*^{ERT2}*/LSL-K-ras*$^{G12D/+}$ mice 6 days and 21 days after induction; Figure S3) and led to the formation of mSH, which did not progress unless *Ink4a/Arf* was deleted. Although $K\text{-}ras^{G12D}$ selectively activates Erk in both SI and colon, OIS was induced only in colon, demonstrating the requirement for expression of so far unidentified coexisting factors other than Erk, that regulate senescence in the large intestine, but not in the small intestine. These data also raise the question how valid certain animals models are concerning colorectal tumor development, in case these models develop tumors only in small intestine.

To date no other genetic model addressing the function of oncogenic K-ras in the intestine has addressed the development of serrated tumorigenesis. Recent reports demonstrated the occurrence of colonic hyperplasia in mice expressing the same $K\text{-}ras^{G12D}$ mutant, however, serrated tumors or the existence of OIS were not described (Haigis et al., 2008; Trobridge et al., 2009). Furthermore, other studies analyzing the function of intestinal K-ras made use of a transgenic approach (Janssen et al., 2006; Janssen et al., 2002), which—albeit moderate overexpression levels of oncogenic K-ras—might lead to the activation of additional downstream signaling cascades. Moreover, when K-ras was activated using an endogenous $K\text{-}ras^{V12}$ mutant, Cre-recombinase was expressed under the control of a promoter that is preferentially expressed in small intestine (Ireland et al., 2004; Sansom et al., 2006), which could account for the different phenotypes regarding the colon. Nevertheless, concerning the K-ras mediated hyperproliferative phenotype in small intestine and in respect to concomitant activation of oncogenic K-ras along with Wnt signaling in either small or large intestine, our data are in agreement with other reports (Haigis et al., 2008; Janssen et al., 2006; Sansom et al., 2006).

Interestingly, murine and human serrated tumors consistently displayed nuclear p53 accumulation in the absence of somatic *TP53* mutations. Especially in case of *K-ras*^{G12Dint}*/Ink4a/Arf*$^{-/-}$ mice this finding was unexpected because $p19^{Arf}$ can function as an upstream activator of p53. Although the functional relevance of this upregulation remains speculative, p53 may not be an important tumor suppressor in our model because IEC-specific deletion of *Tp53* in *K-ras*^{G12Dint} mice did not induce progression of serrated hyperplasia. Moreover, when *Tp53* was inactivated in IEC of *K-ras*^{G12Dint}*/Ink4a/Arf*$^{-/-}$ mice, tumor progression was not further enhanced when compared to *K-ras*^{G12Dint}*/Ink4a/Arf*$^{-/-}$ mice alone. Although $p19^{Arf}$ can mediate certain functions independently of p53, our data strongly suggest that the $p16^{ink4a}$/Rb and not the $p19^{Arf}$/p53 pathway mediate senescence in *K-ras*^{G12Dint} mice.

In summary, we provide evidence that oncogenic K-ras activation represents a key event during early Wnt-independent serrated tumorigenesis in mice and suggest that upregulation of $p16^{INK4A}$ and induction of OIS is a common phenomenon in human *KRAS* mutated serrated tumor development. Thus, we propose that loss of $p16^{INK4A}$ function for example by promoter methylation can be one possibility to overcome senescence thereby allowing tumor progression along the alternative, serrated route. Although there is no doubt anymore that benign serrated lesions can progress into malignant stages, it remains an important task to unravel useful markers that distinguish those polyps that are likely to progress to cancer. Our mouse model may represent an excellent tool to identify some of them.

EXPERIMENTAL PROCEDURES

Mice and Induction of Colonic Tumors

To express K-ras^{G12D} in enterocytes, we crossed *LSL-K-ras^{G12D}* (Hingorani et al., 2003) to *villin-Cre* mice (both on a C57BL/6;129 background)(Madison et al., 2002). *Ink4a/Arf* null (FVB/N.129) (Serrano et al., 1996) were obtained from the MMHC, National Cancer Institute. *K-ras^{G12Dint}* mice were backcrossed for four generations on a FVB background before they were intercrossed with *Ink4a/Arf* null mice. Activation of K-ras^{G12D} in *villin-cre^{ERT2}/LSL-K-ras$^{G12D/+}$* mice was achieved by five daily oral administrations of 1 mg tamoxifen in an ethanol/sunflower oil mixture. Six- to eight-week-old mice (*LSL-K-ras^{G12D}* and *K-ras^{G12Dint}*) were injected i.p. with 15 mg/kg AOM (NCI) once a week for 6 weeks. Sixteen weeks after the first injection animals were sacrificed, colons were removed and analyzed as described (Greten et al., 2004). In all experiments littermate controls were used assuring comparison of mice on the same genetic background. All procedures conformed to the regulatory standards and were approved by the Regierung von Oberbayern. All human samples were obtained with the approval of the ethics committee of the Technical University of Munich from subjects that had given their written informed consent.

Determination of Proliferation and Migration Rates

Mice were injected i.p. with 100 mg/kg BrdU (Sigma) 1.5 hr before sacrifice and paraffin sections were stained using α-BrdU antibody (Amersham Bioscience RPN201). For determination of migration rates, BrdU-injected mice were sacrificed after 48 hr. For each analysis BrdU-positive cells were scored in 12 full crypts from two to five animals of each genotype.

MSI and Methylation Analysis

For examination of murine tissues PCR-based amplification of five microsatellite repeat markers (Kabbarah et al., 2003) was performed using DNA isolated from tumor tissue as well as healthy livers of the corresponding animals. For analysis of human tissue mononucleotide markers BAT25 and BAT26 were used (Deschoolmeester et al., 2008). Fluorescent PCR products were analyzed by capillary electrophoresis using an ABI 3100 Genetic Analyzer (Applied Biosystems) and 3130 Data Collection v3.0 software. Methylated DNA immunoprecipitation and hybridization on a NimbleGen 385K MM8 RefSeq promoter array was performed by imaGenes (GmbH, Berlin).

Laser Capture Microdissection

Laser capture microdissection and sequencing analysis of exon 3 of *Ctnnb* and exons 5–8 of *Tp53* were performed as described previously (Greten et al., 2004).

Senescence Assay

Tissue was fixed in 4% paraformaldehyde for 2 hr on ice, washed twice with PBS, and kept in 15% sucrose solution for 4 hr followed by an overnight incubation in 30% sucrose at 4°C. Samples were embedded in OCT and shock-frozen. SA-β-galactosidase staining was performed on 6-μm cryosections using the Senescence β-galactosidase staining kit (Cell Signaling 9860) according to the manufacturer's instructions.

Protein Analysis

Isolation of enterocytes, immunoblot analysis, and immune complex kinase assay were essentially performed as described (Bollrath et al., 2009). Ras and Ral activation assays were performed using the Ras Activation Assay Kit (Upstate 17-218) or Ral Activation Assay kit (Upstate 17-300) according to the manufacturer's instructions. The following antibodies were used in immunoblot analysis: α-phospho-Erk (9101), α-phospho-p38 (9211), α-phospho-Akt (9271), α-Erk1/2 (9102), α-Akt (9272), α-p15^{INK4b} (4822, Cell Signaling), α-Jnk (PharMingen 554286), α-p38 (SC-535), α-p16^{ink4a} (SC-1661), α-p19^{ARF} (Abcam ab80-50), and α-β-actin (A4700, Sigma).

Immunohistochemistry

Paraffin sections (3.5 μm) were stained using standard immunohistochemical procedures. The following antibodies were used for murine tissues: α-cyclin D1 (Santa Cruz SC-718), α-c-*myc* (SC-788), α-β-catenin (UBI 6734), α-p53 (Novocastra CM5), α-cytokeratin8/18 (Progen GP11), α-cytokeratin 7 (Progen 16090), α-cytokeratin 20 (Progen GP-K20), α-thyroid transcription factor-1 (Dako M3575), α-EphB2 (R&D Systems, AF467), α-HIF1α (Novus, NB 100-131) α-CD45 (PharMingen 553089), α-CD3 (BD PharMingen 555274), and α-MUC5AC (Neomarker MS-145). Immunohistochemical analysis of human tissues was performed on a Benchmark XT (Ventana Medical Systems, Inc.) using the following antibodies: α-MLH1 (BD PharMingen 551091), α-MGMT (medac MS-470-P), α-β-catenin (Ventana 760-4242), α-p14^{ARF} (CytoMed Systems Mob456), α-p16^{INK4A} (Diagnostic Biosystems Mob213), and α-p53 (NeoMarkers MS-186-Po).

RNA Analysis

The RNeasy Mini Kit (QIAGEN) was used for RNA extraction of isolated enterocytes. Synthesis of cDNA was performed using SuperScript II Reverse Transcriptase (Invitrogen). Real-time PCR analysis using Power SYBR Green PCR Master Mix (Applied Biosystems) was performed on a StepOne Plus Real-Time PCR system (Applied Biosystems). Primer sequences are available on request. Gene expression profiling of tumor tissue was performed using Affymetrix Gene ST GeneChips as reported before (Eckmann et al., 2008). In gene set enrichment analysis (GSEA) we matched 87 transcripts that were upregulated in *Apc*-deficient IEC (Sansom et al., 2007) to all transcripts from the Affymetrix Mouse Genome 430A 2.0 Array, respectively. GSEA software is provided by Broad Institute of MIT and Harvard University (http://www.broad.mit.edu/gsea). We acknowledge the use of GSEA software (Subramanian et al., 2005) to validate correlation between molecular pathways signatures in any phenotype of interest. For analysis of gene sets we changed default parameters as follows: permutation number to 1000; collapse data set to gene symbols if "false"; gene sets <1 and >2000 were excluded.

Statistical Analysis

Data are expressed as mean ± SEM. Differences were analyzed by unpaired, two-tailed Student's t test using Prism4 (GraphPad Software); p value ≤ 0.05 were considered significant.

ACCESSION NUMBERS

Gene expression raw data is deposited in the GEO database under accession number GSE20647.

SUPPLEMENTAL INFORMATION

Supplemental Information includes four figures and one table and can be found with this article online at doi:10.1016/j.ccr.2010.06.013.

ACKNOWLEDGMENTS

We thank K. Burmeister, I. Redich, A. Sendelhofert, and A. Heier for excellent technical assistance. We are grateful to D. Gumucio for providing *villin-Cre* mice. We thank R. Hoffmann and A. Servatius for generation of microarray data. This work was supported by grants from the AICR (09-0725), Deutsche Forschungsgemeinschaft (Emmy-Noether-Program Gr1916/2-2), and Deutsche Krebshilfe (108872) to F.R.G.

Received: January 24, 2010
Revised: May 4, 2010
Accepted: June 21, 2010
Published: August 16, 2010

REFERENCES

Boivin, G.P., Washington, K., Yang, K., Ward, J.M., Pretlow, T.P., Russell, R., Besselsen, D.G., Godfrey, V.L., Doetschman, T., Dove, W.F., et al. (2003). Pathology of mouse models of intestinal cancer: consensus report and recommendations. Gastroenterology *124*, 762–777.

Boland, C.R., Thibodeau, S.N., Hamilton, S.R., Sidransky, D., Eshleman, J.R., Burt, R.W., Meltzer, S.J., Rodriguez-Bigas, M.A., Fodde, R., Ranzani, G.N., et al. (1998). A National Cancer Institute Workshop on Microsatellite Instability for cancer detection and familial predisposition: development of international

criteria for the determination of microsatellite instability in colorectal cancer. Cancer Res. *58*, 5248–5257.

Bollrath, J., Phesse, T.J., von Burstin, V.A., Putoczki, T., Bennecke, M., Bateman, T., Nebelsiek, T., Lundgren-May, T., Canli, O., Schwitalla, S., et al. (2009). gp130-mediated Stat3 activation in enterocytes regulates cell survival and cell-cycle progression during colitis-associated tumorigenesis. Cancer Cell *15*, 91–102.

Braig, M., Lee, S., Loddenkemper, C., Rudolph, C., Peters, A.H., Schlegelberger, B., Stein, H., Dorken, B., Jenuwein, T., and Schmitt, C.A. (2005). Oncogene-induced senescence as an initial barrier in lymphoma development. Nature *436*, 660–665.

Chen, Z., Trotman, L.C., Shaffer, D., Lin, H.K., Dotan, Z.A., Niki, M., Koutcher, J.A., Scher, H.I., Ludwig, T., Gerald, W., et al. (2005). Crucial role of p53-dependent cellular senescence in suppression of Pten-deficient tumorigenesis. Nature *436*, 725–730.

Collado, M., Gil, J., Efeyan, A., Guerra, C., Schuhmacher, A.J., Barradas, M., Benguria, A., Zaballos, A., Flores, J.M., Barbacid, M., et al. (2005). Tumour biology: senescence in premalignant tumours. Nature *436*, 642.

Collado, M., and Serrano, M. (2010). Senescence in tumours: evidence from mice and humans. Nat. Rev. Cancer *10*, 51–57.

Cunningham, K.S., and Riddell, R.H. (2006). Serrated mucosal lesions of the colorectum. Curr. Opin. Gastroenterol. *22*, 48–53.

Deschoolmeester, V., Baay, M., Wuyts, W., Van Marck, E., Van Damme, N., Vermeulen, P., Lukaszuk, K., Lardon, F., and Vermorken, J.B. (2008). Detection of microsatellite instability in colorectal cancer using an alternative multiplex assay of quasi-monomorphic mononucleotide markers. J. Mol. Diagn. *10*, 154–159.

Dimri, G.P., Lee, X., Basile, G., Acosta, M., Scott, G., Roskelley, C., Medrano, E.E., Linskens, M., Rubelj, I., Pereira-Smith, O., et al. (1995). A biomarker that identifies senescent human cells in culture and in aging skin in vivo. Proc. Natl. Acad. Sci. USA *92*, 9363–9367.

Eckmann, L., Nebelsiek, T., Fingerle, A.A., Dann, S.M., Mages, J., Lang, R., Robine, S., Kagnoff, M.F., Schmid, R.M., Karin, M., et al. (2008). Opposing functions of IKKbeta during acute and chronic intestinal inflammation. Proc. Natl. Acad. Sci. USA *105*, 15058–15063.

el Marjou, F., Janssen, K.P., Chang, B.H., Li, M., Hindie, V., Chan, L., Louvard, D., Chambon, P., Metzger, D., and Robine, S. (2004). Tissue-specific and inducible Cre-mediated recombination in the gut epithelium. Genesis *39*, 186–193.

Greenblatt, M.S., Bennett, W.P., Hollstein, M., and Harris, C.C. (1994). Mutations in the p53 tumor suppressor gene: clues to cancer etiology and molecular pathogenesis. Cancer Res. *54*, 4855–4878.

Greten, F.R., Eckmann, L., Greten, T.F., Park, J.M., Li, Z.W., Egan, L.J., Kagnoff, M.F., and Karin, M. (2004). IKKbeta links inflammation and tumorigenesis in a mouse model of colitis-associated cancer. Cell *118*, 285–296.

Haigis, K.M., Kendall, K.R., Wang, Y., Cheung, A., Haigis, M.C., Glickman, J.N., Niwa-Kawakita, M., Sweet-Cordero, A., Sebolt-Leopold, J., Shannon, K.M., et al. (2008). Differential effects of oncogenic K-Ras and N-Ras on proliferation, differentiation and tumor progression in the colon. Nat. Genet. *40*, 600–608.

Hingorani, S.R., Petricoin, E.F., Maitra, A., Rajapakse, V., King, C., Jacobetz, M.A., Ross, S., Conrads, T.P., Veenstra, T.D., Hitt, B.A., et al. (2003). Preinvasive and invasive ductal pancreatic cancer and its early detection in the mouse. Cancer Cell *4*, 437–450.

Huang, C.S., O'Brien, M.J., Yang, S., and Farraye, F.A. (2004). Hyperplastic polyps, serrated adenomas, and the serrated polyp neoplasia pathway. Am. J. Gastroenterol. *99*, 2242–2255.

Ireland, H., Kemp, R., Houghton, C., Howard, L., Clarke, A.R., Sansom, O.J., and Winton, D.J. (2004). Inducible Cre-mediated control of gene expression in the murine gastrointestinal tract: effect of loss of beta-catenin. Gastroenterology *126*, 1236–1246.

Jackson, E.L., Willis, N., Mercer, K., Bronson, R.T., Crowley, D., Montoya, R., Jacks, T., and Tuveson, D.A. (2001). Analysis of lung tumor initiation and progression using conditional expression of oncogenic K-ras. Genes Dev. *15*, 3243–3248.

Janssen, K.P., Alberici, P., Fsihi, H., Gaspar, C., Breukel, C., Franken, P., Rosty, C., Abal, M., El Marjou, F., Smits, R., et al. (2006). APC and oncogenic KRAS are synergistic in enhancing Wnt signaling in intestinal tumor formation and progression. Gastroenterology *131*, 1096–1109.

Janssen, K.P., el-Marjou, F., Pinto, D., Sastre, X., Rouillard, D., Fouquet, C., Soussi, T., Louvard, D., and Robine, S. (2002). Targeted expression of oncogenic K-ras in intestinal epithelium causes spontaneous tumorigenesis in mice. Gastroenterology *123*, 492–504.

Jass, J.R. (2007). Classification of colorectal cancer based on correlation of clinical, morphological and molecular features. Histopathology *50*, 113–130.

Jass, J.R., Whitehall, V.L., Young, J., and Leggett, B.A. (2002). Emerging concepts in colorectal neoplasia. Gastroenterology *123*, 862–876.

Jemal, A., Siegel, R., Ward, E., Hao, Y., Xu, J., and Thun, M.J. (2009). Cancer statistics, 2009. CA Cancer J. Clin. *59*, 225–249.

Jonkers, J., Meuwissen, R., van der Gulden, H., Peterse, H., van der Valk, M., and Berns, A. (2001). Synergistic tumor suppressor activity of BRCA2 and p53 in a conditional mouse model for breast cancer. Nat. Genet. *29*, 418–425.

Kabbarah, O., Mallon, M.A., Pfeifer, J.D., Edelmann, W., Kucherlapati, R., and Goodfellow, P.J. (2003). A panel of repeat markers for detection of microsatellite instability in murine tumors. Mol. Carcinog. *38*, 155–159.

Kaiser, S., Park, Y.K., Franklin, J.L., Halberg, R.B., Yu, M., Jessen, W.J., Freudenberg, J., Chen, X., Haigis, K., Jegga, A.G., et al. (2007). Transcriptional recapitulation and subversion of embryonic colon development by mouse colon tumor models and human colon cancer. Genome Biol. *8*, R131.

Kamangar, F., Dores, G.M., and Anderson, W.F. (2006). Patterns of cancer incidence, mortality, and prevalence across five continents: defining priorities to reduce cancer disparities in different geographic regions of the world. J. Clin. Oncol. *24*, 2137–2150.

Kinzler, K.W., and Vogelstein, B. (1996). Lessons from hereditary colorectal cancer. Cell *87*, 159–170.

Laiho, P., Kokko, A., Vanharanta, S., Salovaara, R., Sammalkorpi, H., Jarvinen, H., Mecklin, J.P., Karttunen, T.J., Tuppurainen, K., Davalos, V., et al. (2007). Serrated carcinomas form a subclass of colorectal cancer with distinct molecular basis. Oncogene *26*, 312–320.

Lee, H.Y., Suh, Y.A., Lee, J.I., Hassan, K.A., Mao, L., Force, T., Gilbert, B.E., Jacks, T., and Kurie, J.M. (2002). Inhibition of oncogenic K-ras signaling by aerosolized gene delivery in a mouse model of human lung cancer. Clin. Cancer Res. *8*, 2970–2975.

Lengauer, C., Kinzler, K.W., and Vogelstein, B. (1998). Genetic instabilities in human cancers. Nature *396*, 643–649.

Madison, B.B., Dunbar, L., Qiao, X.T., Braunstein, K., Braunstein, E., and Gumucio, D.L. (2002). Cis elements of the villin gene control expression in restricted domains of the vertical (crypt) and horizontal (duodenum, cecum) axes of the intestine. J. Biol. Chem. *277*, 33275–33283.

Makinen, M.J. (2007). Colorectal serrated adenocarcinoma. Histopathology *50*, 131–150.

Malumbres, M., and Barbacid, M. (2003). RAS oncogenes: the first 30 years. Nat. Rev. Cancer *3*, 459–465.

Michaloglou, C., Vredeveld, L.C., Soengas, M.S., Denoyelle, C., Kuilman, T., van der Horst, C.M., Majoor, D.M., Shay, J.W., Mooi, W.J., and Peeper, D.S. (2005). BRAFE600-associated senescence-like cell cycle arrest of human nevi. Nature *436*, 720–724.

Mooi, W.J., and Peeper, D.S. (2006). Oncogene-induced cell senescence—halting on the road to cancer. N. Engl. J. Med. *355*, 1037–1046.

Noffsinger, A.E. (2009). Serrated polyps and colorectal cancer: new pathway to malignancy. Annu. Rev. Pathol. *4*, 343–364.

Sansom, O.J., Meniel, V., Wilkins, J.A., Cole, A.M., Oien, K.A., Marsh, V., Jamieson, T.J., Guerra, C., Ashton, G.H., Barbacid, M., et al. (2006). Loss of Apc allows phenotypic manifestation of the transforming properties of an endogenous K-ras oncogene in vivo. Proc. Natl. Acad. Sci. USA *103*, 14122–14127.

Sansom, O.J., Meniel, V.S., Muncan, V., Phesse, T.J., Wilkins, J.A., Reed, K.R., Vass, J.K., Athineos, D., Clevers, H., and Clarke, A.R. (2007). Myc deletion rescues Apc deficiency in the small intestine. Nature *446*, 676–679.

Serrano, M., Lee, H., Chin, L., Cordon-Cardo, C., Beach, D., and DePinho, R.A. (1996). Role of the INK4a locus in tumor suppression and cell mortality. Cell *85*, 27–37.

Subramanian, A., Tamayo, P., Mootha, V.K., Mukherjee, S., Ebert, B.L., Gillette, M.A., Paulovich, A., Pomeroy, S.L., Golub, T.R., Lander, E.S., et al. (2005). Gene set enrichment analysis: a knowledge-based approach for interpreting genome-wide expression profiles. Proc. Natl. Acad. Sci. USA *102*, 15545–15550.

Trobridge, P., Knoblaugh, S., Washington, M.K., Munoz, N.M., Tsuchiya, K.D., Rojas, A., Song, X., Ulrich, C.M., Sasazuki, T., Shirasawa, S., et al. (2009). TGF-beta receptor inactivation and mutant Kras induce intestinal neoplasms in mice via a beta-catenin-independent pathway. Gastroenterology *136*, 1680–1688.

Vogelstein, B., Fearon, E.R., Hamilton, S.R., Kern, S.E., Preisinger, A.C., Leppert, M., Nakamura, Y., White, R., Smits, A.M., and Bos, J.L. (1988). Genetic alterations during colorectal-tumor development. N. Engl. J. Med. *319*, 525–532.

Weisenberger, D.J., Siegmund, K.D., Campan, M., Young, J., Long, T.I., Faasse, M.A., Kang, G.H., Widschwendter, M., Weener, D., Buchanan, D., et al. (2006). CpG island methylator phenotype underlies sporadic microsatellite instability and is tightly associated with BRAF mutation in colorectal cancer. Nat. Genet. *38*, 787–793.